2024 IEEE International Conference on Robotics and Automation (ICRA 2024)
May 13-17, 2024. Yokohama, Japan

Relaxed Hover Solution Based Control for a Bi-copter with Rotor and Servo Stuck Failure

Haixin Zhao, Ruifeng Li, Quan Quan*

***Abstract*— As the usage of bi-copters increases in military and civilian fields, the demand for reliable bi-copters is on the rise. This study focuses on controlling a bi-copter under rotor or servo stuck failure. A relaxed hover solution is derived for the bi-copter, by solving an optimization problem subject to rotor and servo stuck failures. The solution is used for designing a reduced attitude controller based on linear quadratic regulator (LQR). To ensure hover capability, we introduce a position controller based on a cascaded-PID. The numerical simulations are conducted to demonstrate that position control is possible, even with complete rotor or servo stuck failure, by driving the bi-copter into relaxed hover state through the abandonment of the yaw channel. Meanwhile, the FTC scheme is examined under constant wind disturbances and uncertainties in the rotational damping parameters.**

I. Introduction

Over the past decade, multicopters have become ubiquitous in our daily lives [1]. Recently, bi-copters have been gaining popularity in agriculture and photography. Unlike multicopters, bi-copters have fewer rotors, which means less redundancy in the propulsion system. This makes their fault tolerant control (FTC) more challenging. Besides the rotor failure, the servos stuck failure (e.g., [2],[3],[4]) is another safety problem for bi-copters. With the increasing deployment of bi-copters, it is crucial to improve their safety and reliability. However, there is a lack of relevant research on the topic.

A bi-copter is equipped with four actuators. It uses two rotors to produce lift force and two servos to tilt the rotors. The bi-copter flies forward or backward by tilting rotors in the same direction, while pitch torque is generated simultaneously. Tilted rotors in opposite directions generate torque in the yaw channel. Similar to multicopters, roll torque is generated by the different thrusts of the two rotors. Moreover, some studies focus on a bi-copter with wings (e.g., [5] and [6]). This type of bi-copters is classified as hybrid UAVs in [7]. This study mainly focuses on a bi-copter without wings, shown in Fig. 1. It features on its compact size and efficiency [8].

FTC is a challenge in UAVs for its applications. The majority of studies focus on multicopters. A relaxed hover solution for multicopters is derived in [9]. The solution is an equilibrium point where the multicopter gives up yaw control to keep altitude and horizontal position controllable.

Haixin Zhao, Ruifeng Li, Quan Quan (Corresponding Author) are with School of Automation Science and Electrical Engineering, Beihang University, Beijing, 100191, P.R. China hx_zhao@buaa.edu.cn, liruifeng5@buaa.edu.cn, qq_buaa@buaa.edu.cn

This work was supported by the National Natural Science Foundation of China under Grant 61973015.

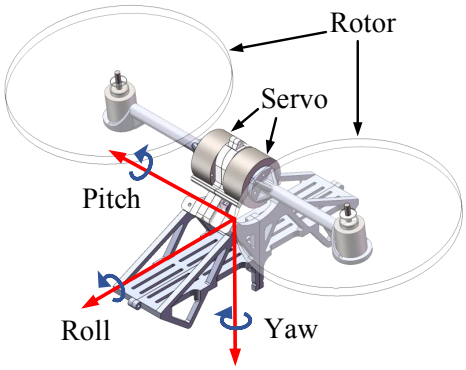

Fig. 1. 3D Model of a Bi-copter

The study demonstrates the possibility of flying a quadcopter despite complete rotor failure. Furthermore, a uniform passive FTC scheme of quadcopters subject to one, two, or three rotor failure is proposed in [10]. It is worth noting that the rotors' failure is modeled as a disturbance. As a result, the rotor failure information is unnecessary for FTC. Another study [11] focuses on a failed quadcopter performing upset recovery from extreme initial conditions and tracking agile trajectories. Regarding a hexarotor with rotor failure, the studies by [12] and [13] are relevant.

It is worth noting that the inertia parameters of UAVs significantly influence their controllability in a self-rotation state, as described in [14]. For the single rotor vehicle in [15], the inertia parameters were meticulously designed using Monte Carlo analysis to ensure sufficient robustness. Similar results can also be observed for quadcopters in [16]. *Both of them resemble spinning disks with natural stability* [17]. However, in our platform, the maximum inertia channel of the bi-copter is around roll, while the minimum is around pitch. A significant roll torque is generated when the bi-copter suffers a rotor failure, causing undesired rolling. Additionally, a tiltable thrust direction leads to a more complex control method, but offers greater potential for FTC. These make FTC more challenging on a bi-copter. Overall, to the best of our knowledge, there is no study on the FTC of bi-copters subject to rotor or servo stuck failure.

This paper focuses on controlling a bi-copter subject to a rotor or servo stuck failure, aiming to indicate the feasibility of position control. Firstly, we establish the dynamics model and failure model of the bi-copter. Then, we derive a relaxed hover solution [9] for the bi-copter, the reduced attitude controller and position controller are presented as well. Finally, numerical simulations of a controllable bi-

copter with a failed rotor or servo are demonstrated. The contributions of this paper are summarized as two aspects.

- A relaxed hover solution for a bi-copter is derived for the first time. An optimization problem is formulated to obtain the solution, considering actuator limitation. Both rotor and servo failure are accommodated by the scheme.
- Based on the solution, a position controller is designed with simulation to show the effectiveness.

II. Problem Formulation

A. Modeling

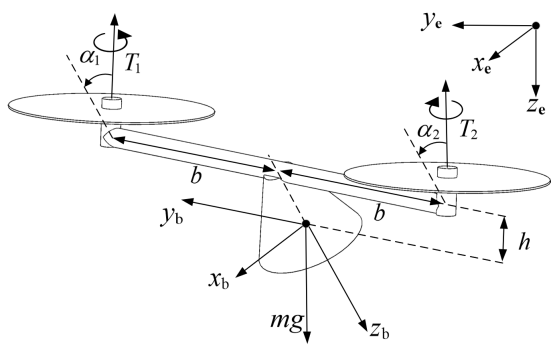

Fig. 2. Diagram of a Bi-copter

Referring to Fig. 2 for a diagram of the bi-copter, the body frame $\{x_\mathrm{b}, y_\mathrm{b}, z_\mathrm{b}\}$ and the Earth frame $\{x_\mathrm{e}, y_\mathrm{e}, z_\mathrm{e}\}$ both follow the right-handed coordinate system. The origin of the body frame, denoting the center of mass of the bi-copter, is displayed in the diagram. Vector $\mathbf{g} = \begin{bmatrix}0 & 0 & g\end{bmatrix}^\mathrm{T}$ is the acceleration vector of the gravity in the Earth frame. The attitude of the bi-copter is described by Direction Cosine Matrix (DCM) denoted as $\mathbf{R}_\mathrm{eb} \in \mathbb{R}^{3\times3}$. The attitude $\mathbf{R}_\mathrm{eb}$ describes the rotation from the body frame to the Earth frame. Vector $\mathbf{p} \in \mathbb{R}^3$ denotes the position of the bi-copter in the Earth frame, and its velocity is expressed as $\mathbf{v} \in \mathbb{R}^3$. The angular velocity, denoted by $\boldsymbol{\omega} = \begin{bmatrix}p & q & r\end{bmatrix}^\mathrm{T} \in \mathbb{R}^3$, is expressed in the body frame. The dynamics equations of bi-copter are

$$\begin{aligned}
\dot{\mathbf{p}} &= \mathbf{v} \\
\dot{\mathbf{v}} &= \mathbf{g} + \frac{1}{m}\mathbf{R}_\mathrm{eb}\mathbf{f} + \frac{1}{m}\mathbf{d}_\mathrm{linear} \\
\dot{\mathbf{R}}_\mathrm{eb} &= \mathbf{R}_\mathrm{eb}[\boldsymbol{\omega}]_\times \\
\mathbf{J}\dot{\boldsymbol{\omega}} &= \boldsymbol{\tau} + \mathbf{d}_\mathrm{rot} - \boldsymbol{\omega} \times (\mathbf{J}\boldsymbol{\omega}),
\end{aligned} \tag{1}$$

where

$$\begin{aligned}
\mathbf{f}_i &= \begin{bmatrix} f_{i,x} \\ f_{i,y} \\ f_{i,z} \end{bmatrix} = \begin{bmatrix} T_i \sin(\alpha_i) \\ 0 \\ T_i \cos(\alpha_i) \end{bmatrix}, \\
\boldsymbol{\tau}_i &= \mathbf{l}_i \times \mathbf{f}_i + (-1)^i k_\tau \mathbf{f}_i, \qquad i = 1, 2 \\
\mathbf{f} &= \mathbf{f}_1 + \mathbf{f}_2, \quad \boldsymbol{\tau} = \boldsymbol{\tau}_1 + \boldsymbol{\tau}_2,
\end{aligned} \tag{2}$$

and

$$[\boldsymbol{\omega}]_\times = \begin{bmatrix} 0 & -r & q \\ r & 0 & -p \\ -q & p & 0 \end{bmatrix}. \tag{3}$$

The matrix $\mathbf{J} = \mathrm{diag}\,(J_x, J_y, J_z) \in \mathbb{R}^{3\times3}$, assumed to be diagonal when expressed in the body frame, represents the entire inertia of the bi-copter; T_i is the force generated by the *i*-th rotor; α_i is the tilt angle of the *i*-th servo related to the $-z_\mathrm{b}$ axis. The rotation around the $-y_\mathrm{b}$ axis is defined as the positive direction of α_i. The vector $\mathbf{f}_i$ and $\boldsymbol{\tau}_i$ are the force and torque generated by *i*-th rotor in the body frame. The scalar k_τ represents the torque coefficient of the rotor [18]. The length of the arm is denoted as b; the height of the servo axis above the center of mass is represented by h; vector $\mathbf{l}_i$ is the *i*-th rotor position in the body frame, $\mathbf{l}_i = \begin{bmatrix}0 & (-1)^{i+1}b & -h\end{bmatrix}^\mathrm{T}$. Term $\mathbf{d}_\mathrm{linear} \in \mathbb{R}^3$ represents the disturbances expressed in the Earth frame, such as wind disturbances; the term $\mathbf{d}_\mathrm{rot} \in \mathbb{R}^3$ represents the drag force generated by the bi-copter's angular motion. In study [9], the air drag is modeled as

$$\mathbf{d}_\mathrm{rot} = -\|\boldsymbol{\omega}\|\mathbf{k}_\mathrm{air}\boldsymbol{\omega}, \tag{4}$$

where $\mathbf{k}_\mathrm{air} = \mathrm{diag}\,(k_x, k_y, k_z) \in \mathbb{R}^{3\times3}$. Due to the dynamics of the rotors, the thrust generated by the rotor cannot track the commanded thrust without delay. A first-order inertial model is adopted to approximate the behavior of a real rotor, namely

$$\tau_\mathrm{m}\dot{T}_i = T_{\mathrm{c},i} - T_i, \quad T_{\mathrm{c},i} \in \left[0, \quad \lambda_i T_{\mathrm{max},i}\right], \tag{5}$$

where the rotor's actual thrust is T_i; $T_{\mathrm{c},i}$ represents the commanded thrust generated by the controller; τ_m is the rotor's time constant indicating the bandwidth of the rotor; $T_{\mathrm{max},i}$ is the maximum thrust of *i*-th rotor; λ_i is the efficiency coefficient, $0 \le \lambda_i \le 1$. In particular, the *i*-th rotor fails entirely, when $\lambda_i = 0$. Similar to the rotor, the tilt servo is also considered as a first-order inertial model, namely

$$\tau_\mathrm{s}\dot{\alpha}_i = \alpha_{\mathrm{c},i} - \alpha_i, \quad \alpha_{\mathrm{c},i} \in \left[\alpha_{\mathrm{min},i}, \alpha_{\mathrm{max},i}\right]. \tag{6}$$

The time constant of the tilt servo is denoted as τ_s, and $\alpha_{\mathrm{c},i}$ represents the commanded angle of the *i*-th servo. The minimum and maximum limits of the *i*-th servo are represented by $\alpha_{\mathrm{min},i}$ and $\alpha_{\mathrm{max},i}$, respectively. When the failure of *i*-th servo occurs, $\alpha_{\mathrm{min},i} = \alpha_{\mathrm{max},i} = \alpha_{\mathrm{fault},i}$, where $\alpha_{\mathrm{fault},i}$ denotes as the position of stuck angle of *i*-th servo. Note that the non-minimum phase dynamics and the augular momentum of the rotors are ignored. Typically, the bi-copter has four command inputs, namely

$$\mathbf{u} \triangleq \begin{bmatrix}T_{\mathrm{c},1} & T_{\mathrm{c},2} & \alpha_{\mathrm{c},1} & \alpha_{\mathrm{c},2}\end{bmatrix}^\mathrm{T}. \tag{7}$$

The system outputs are $\begin{bmatrix}\mathbf{p}^\mathrm{T} & \mathbf{v}^\mathrm{T} & \boldsymbol{\omega}^\mathrm{T}\end{bmatrix}^\mathrm{T}$ and $\mathbf{R}$, and these states could be measured or fused to obtain.

B. Objective

The control objective is to achieve efficient position control of a failed bi-copter, namely $\lim_{t\to\infty} \|\mathbf{p}_\mathrm{d}(t) - \mathbf{p}(t)\| = 0$, subject to $\lambda_2 \in [0, 1]$ or $\alpha_{\mathrm{min},2} = \alpha_{\mathrm{max},2} = \alpha_{\mathrm{fault},2}$, where $\mathbf{p}_\mathrm{d}$

is the desired position. The objective implies that the failed bi-copter could maintain its position in the space rather than crashing. It is worth noting that this paper does not include fault detection and diagnosis, as other studies have already focused on this topic (e.g., [19],[20]).

III. Controller Design

Similar to multicopters, the failed bi-copter must keep the desired altitude to avoid crashing. We can abandon the yaw control to achieve that. If the bi-copter tracks the desired acceleration in average acceleration during self-rotation rather than instantaneous acceleration, it indicates that the bi-copter is in *relaxed hover solution*. To achieve that, a controller scheme is described in this section.

A. Relaxed-Hover Solution of Bi-copter

We define that the self-rotation period is $\overline{T} \triangleq \frac{2\pi}{\|\overline{\boldsymbol{\omega}}\|}$, where $\overline{(\cdot)}$ represents that the system state is in equilibrium condition. From (1), under the equilibrium condition, the linear dynamics equation is rewritten as

$$\frac{1}{\overline{T}}\int_0^{\overline{T}} m\dot{\mathbf{v}}\mathrm{d}t = \frac{1}{\overline{T}}\int_0^{\overline{T}} (\mathbf{R}_{\text{eb}}(t)\mathbf{f} + m\mathbf{g})\mathrm{d}t. \tag{8}$$

Note that $\mathbf{d}_{\text{linear}}$ is ignored in the derivation. Substituting $\mathbf{R}_{\text{eb}}(t) = \mathbf{R}_{\text{eb}}(0)e^{[\boldsymbol{\omega}]_\times t}$ into (8) results in

$$\frac{1}{\overline{T}}\int_0^{\overline{T}} m\dot{\mathbf{v}}\mathrm{d}t = \frac{1}{\overline{T}}\mathbf{R}_{\text{eb}}(0)\left(\int_0^{\overline{T}} e^{[\boldsymbol{\omega}]_\times t}\mathrm{d}t\right)\mathbf{f} + m\mathbf{g}. \tag{9}$$

Note that the rotation $\mathbf{R}_{\text{eb}}(t)$ is derived with a constant angular velocity $\boldsymbol{\omega}$. Let $\boldsymbol{\omega} = \overline{\boldsymbol{\omega}}$, and utilizing Rodrigues' formula [21], Equ. (9) is derived as

$$\begin{aligned}\frac{1}{\overline{T}}\int_0^{\overline{T}} m\dot{\mathbf{v}}\mathrm{d}t =& \mathbf{R}_{\text{eb}}(0)\frac{\boldsymbol{\omega}}{\|\boldsymbol{\omega}\|^2}(p(f_{1,x}+f_{2,x}) - r(f_{1,z}+f_{2,z})) \\ &+ m\mathbf{g}.\end{aligned} \tag{10}$$

Let the left-hand side of (10) equal to the desired acceleration $\mathbf{a}_{\text{d}}$. We have

$$\begin{aligned}\mathcal{L}_1 =& \mathbf{R}_{\text{eb}}(0)\frac{\boldsymbol{\omega}}{\|\boldsymbol{\omega}\|^2}(p(f_{1,x}+f_{2,x}) - r(f_{1,z}+f_{2,z})) \\ &+ m\mathbf{g} - m\mathbf{a}_{\text{d}}.\end{aligned} \tag{11}$$

The attitude $\mathbf{R}_{\text{eb}}(0)$ represents the initial attitude during self-rotation. It could also be derived from ZYX Euler angles, namely $\mathbf{R}_{\text{eb}}(0) = \mathbf{R}_{\text{eb}}(\psi(0), \theta(0), \phi(0))$, where ψ, θ, ϕ denote as yaw, pitch and roll. According to (11), let $\mathcal{L}_1 = \mathbf{0}$, the average acceleration equals to desired acceleration $\mathbf{a}_{\text{d}}$ under relaxed hover condition. However, only (11) is not enough. To keep the stable roll and pitch angle, another constraint of angular acceleration is introduced. From (1), we have

$$\mathcal{L}_2 = \dot{\boldsymbol{\omega}} = \mathbf{J}^{-1}(\boldsymbol{\tau} + \mathbf{d}_{\text{rot}} - \boldsymbol{\omega}\times(\mathbf{J}\boldsymbol{\omega})). \tag{12}$$

Equ. (12) indicates that a stable attitude is expected when $\mathcal{L}_2 = \mathbf{0}$. Considering execution time and parameter uncertainty, formulating them as a minimization problem is more suitable than solving algebraic equations. Therefore, the relaxed hover solution could be obtained by minimizing Equ. (11) and Equ. (12), namely

$$\begin{aligned}\overline{\boldsymbol{\gamma}} =& \arg\min_{\boldsymbol{\gamma}} \ \| \mathcal{L}_1 \|^2_{\mathbf{W}_1} + \| \mathcal{L}_2 \|^2_{\mathbf{W}_2} \\ &\text{s.t.} \quad \boldsymbol{\gamma}_{\text{min}} \le \boldsymbol{\gamma} \le \boldsymbol{\gamma}_{\text{max}},\end{aligned} \tag{13}$$

where $\boldsymbol{\gamma} \triangleq \begin{bmatrix}\psi & \theta & \phi & \boldsymbol{\omega}^{\text{T}} & T_1 & T_2 & \alpha_1 & \alpha_2\end{bmatrix}^{\text{T}}$ and $\overline{\boldsymbol{\gamma}} \in \mathbb{R}^{10}$ is the relaxed hover solution. Note that a state constraint for the solution is introduced by γ_{min} and γ_{max}, aiming to acquire an acceptable solution. Both $\mathbf{W}_1 \in \mathbb{R}^{3\times3}$ and $\mathbf{W}_2 \in \mathbb{R}^{3\times3}$ are weight matrices used to control errors for Equ. (11) and Equ. (12). Note that an initial solution $\boldsymbol{\gamma}_{\text{init}} \in \mathbb{R}^{10}$ is provided as an iteration initial value before solving the optimization problem. While a suitable $\boldsymbol{\gamma}_{\text{init}}$ would aid in problem-solving, in the presence of parameter uncertainty, a predefined initial solution may not always be appropriate. In this study, the system state is fed as the initial solution once stable self-rotation is achieved, namely

$$\boldsymbol{\gamma}_{\text{init}} = \begin{cases} \overline{\boldsymbol{\gamma}}_0, & |{}^{\text{e}}n_{\text{z}}| \le \epsilon \\ \boldsymbol{\gamma}_{\text{feedback}}, & |{}^{\text{e}}n_{\text{z}}| > \epsilon \end{cases}. \tag{14}$$

The selection strategy for $\boldsymbol{\gamma}_{\text{init}}$ is depicted in (14), where $\overline{\boldsymbol{\gamma}}_0 \in \mathbb{R}^{10}$ represents the predefined relaxed hover solution satisfying $\mathcal{L}_1 = \mathbf{0}$ and $\mathcal{L}_2 = \mathbf{0}$, $\boldsymbol{\gamma}_{\text{feedback}} \in \mathbb{R}^{10}$ is the initial solution obtained from the current system state, and $\epsilon \in [0, 1]$ is a threshold for switching.

B. Reduced Attitude System

In Section III-A, we address an optimization problem in the form of Equ. (13) and obtain the relaxed hover solution $\overline{\boldsymbol{\gamma}}$. In this section, we present the design of a reduced attitude system utilizing $\overline{\boldsymbol{\gamma}}$ as the bi-copter's equilibrium point. In the relaxed hover mode, the bi-copter rotates with a significant angular velocity $\|\boldsymbol{\omega}\| \gg 0$ and the yaw angle increases. Thus, the traditional attitude representation (e.g., Euler angle or rotation matrix) is not suitable. To address this issue, we adopt the *average thrust direction* [9], namely

$$\mathbf{n} = \frac{\boldsymbol{\omega}}{\|\boldsymbol{\omega}\|}. \tag{15}$$

The vector $\mathbf{n}$ indicates the *average thrust direction* of the bi-copter during self-rotation, and it is a unit vector of the self-rotation axis expressed in the body frame. A new coordinate frame $\{x_{\text{c}}, y_{\text{c}}, z_{\text{c}}\}$ called *control coordinate frame* [9] is introduced, and axis z_{c} coincides with $\overline{\mathbf{n}}$. The rotation matrix $\mathbf{R}_{\text{cb}} \in \mathbb{R}^{3\times3}$ from the body frame to the *control coordinate frame* satisfies

$${}^{\text{c}}\mathbf{n} = \mathbf{R}_{\text{cb}}\overline{\mathbf{n}} = \begin{bmatrix}0 & 0 & 1\end{bmatrix}^{\text{T}}, \tag{16}$$

and $\mathbf{R}_{\text{cb}}$ is determined by

$$\mathbf{R}_{\text{cb}} = \mathbf{I}_3 + [\overline{\mathbf{n}} \times^{\text{c}} \mathbf{n}]_\times + [\overline{\mathbf{n}} \times^{\text{c}} \mathbf{n}]^2_\times \frac{1}{1 + \overline{\mathbf{n}}^{\text{T}}{}^{\text{c}}\mathbf{n}}. \tag{17}$$

So, the angular velocity in the *control coordinate frame* is

$${}^{\text{c}}\boldsymbol{\omega} = \mathbf{R}_{\text{cb}}\boldsymbol{\omega}. \tag{18}$$

Substituting the $\overline{\boldsymbol{\omega}}$ into (18) results in

$${}^{\text{c}}\overline{\boldsymbol{\omega}} = \mathbf{R}_{\text{cb}}\overline{\boldsymbol{\omega}} = \begin{bmatrix}0 & 0 & \|\overline{\boldsymbol{\omega}}\|\end{bmatrix}^{\text{T}}. \tag{19}$$

Furthermore, the desired average thrust direction ${}^{\mathrm{e}}\mathbf{n}_{\mathrm{d}}$ expressed in the *control coordinate frame* is written as

$$ {}^{\mathrm{c}}\mathbf{n}_{\mathrm{d}} = \mathbf{R}_{\mathrm{cb}}\mathbf{R}_{\mathrm{be}}{}^{\mathrm{e}}\mathbf{n}_{\mathrm{d}} = \mathbf{R}_{\mathrm{ce}}{}^{\mathrm{e}}\mathbf{n}_{\mathrm{d}}. \tag{20} $$

The original control is to drive ${}^{\mathrm{e}}\mathbf{n} = \mathbf{R}_{\mathrm{eb}}\mathbf{n} \triangleq \begin{bmatrix}{}^{\mathrm{e}}n_x & {}^{\mathrm{e}}n_y & {}^{\mathrm{e}}n_z\end{bmatrix}^{\mathrm{T}}$ tracking ${}^{\mathrm{e}}\mathbf{n}_{\mathrm{d}}$, defined in the Earth frame. However, the new objective is redefined as making the vector ${}^{\mathrm{c}}\mathbf{n}_{\mathrm{d}}$ stabilizing to ${}^{\mathrm{c}}\mathbf{n} = \begin{bmatrix}0 & 0 & 1\end{bmatrix}^{\mathrm{T}}$ in the control coordinate frame, meaning that the *average thrust direction* ${}^{\mathrm{c}}\mathbf{n}_{\mathrm{d}}$ aligns with ${}^{\mathrm{c}}\mathbf{n}$. A two degrees of freedom attitude system is established. As a result, the kinematics equation of ${}^{\mathrm{c}}\mathbf{n}_{\mathrm{d}}$ is derived as

$$ {}^{\mathrm{c}}\dot{\mathbf{n}}_{\mathrm{d}} = \dot{\mathbf{R}}_{\mathrm{ce}}{}^{\mathrm{e}}\mathbf{n}_{\mathrm{d}} + \mathbf{R}_{\mathrm{ce}}{}^{\mathrm{e}}\dot{\mathbf{n}}_{\mathrm{d}}. \tag{21} $$

Term ${}^{\mathrm{e}}\mathbf{n}_{\mathrm{d}}$ represents the output of position control, whose dynamics are slower than attitude controller. Thus, assuming that ${}^{\mathrm{e}}\mathbf{n}_{\mathrm{d}}$ is close to the constant vector, and term ${}^{\mathrm{e}}\dot{\mathbf{n}}_{\mathrm{d}}$ could be ignored. ${}^{\mathrm{e}}\mathbf{n}_{\mathrm{d}}$ changes more slowly than ${}^{\mathrm{c}}\mathbf{n}_{\mathrm{d}}$ due to attitude coupling. Thus, Equ.(21) is rewritten as

$$ {}^{\mathrm{c}}\dot{\mathbf{n}}_{\mathrm{d}} = \dot{\mathbf{R}}_{\mathrm{ec}}^{\mathrm{T}}{}^{\mathrm{e}}\mathbf{n}_{\mathrm{d}} = \left(\mathbf{R}_{\mathrm{ec}}\left[{}^{\mathrm{c}}\boldsymbol{\omega}\right]_{\times}\right)^{\mathrm{T}}{}^{\mathrm{e}}\mathbf{n}_{\mathrm{d}} = -\left[{}^{\mathrm{c}}\boldsymbol{\omega}\right]_{\times}{}^{\mathrm{c}}\mathbf{n}_{\mathrm{d}}. \tag{22} $$

To obtain the dynamics equation of ${}^{\mathrm{c}}\dot{\boldsymbol{\omega}}$, we approximate it by ${}^{\mathrm{c}}\dot{\boldsymbol{\omega}} = \dot{\boldsymbol{\omega}}$.

C. LQR Controller

Section III-B describes a reduced attitude representation and its dynamics equation. Moreover, a Linear Quadratic Regulator (LQR) [22] based control law is employed to regulate the reduced attitude system. Let ${}^{\mathrm{c}}\mathbf{n}_{\mathrm{d}} \triangleq \begin{bmatrix}\eta_1 & \eta_2 & \eta_3\end{bmatrix}^{\mathrm{T}}$ and ${}^{\mathrm{c}}\boldsymbol{\omega} \triangleq \begin{bmatrix}{}^{\mathrm{c}}p & {}^{\mathrm{c}}q & {}^{\mathrm{c}}r\end{bmatrix}^{\mathrm{T}}$. According to (1),(5),(6),(18),(22), we choose the system state variable as

$$ \mathbf{x} \triangleq \begin{bmatrix}\eta_1 & \eta_2 & {}^{\mathrm{c}}p & {}^{\mathrm{c}}q & {}^{\mathrm{c}}r & T_1 & T_2 & \alpha_1 & \alpha_2\end{bmatrix}^{\mathrm{T}}. \tag{23} $$

The system dynamics equation of $\mathbf{x}$ is formulated as

$$ \dot{\mathbf{x}} = \mathbf{f}(\mathbf{x}, \mathbf{u}). \tag{24} $$

Then, the error state $\Delta\mathbf{x}$ between the state $\mathbf{x}$ and equilibrium state $\overline{\mathbf{x}}$ is defined as $\Delta\mathbf{x} = \mathbf{x} - \overline{\mathbf{x}}$; the error control input is defined as $\Delta\mathbf{u} = \mathbf{u} - \overline{\mathbf{u}}$, where $\overline{\mathbf{u}} = \begin{bmatrix}\overline{T}_1 & \overline{T}_2 & \overline{\alpha}_1 & \overline{\alpha}_2\end{bmatrix}^{\mathrm{T}}$. Note that term $\overline{\mathbf{x}}$ is a constant value, and the differential equation of $\Delta\mathbf{x}$ could be derived directly, namely

$$ \Delta\dot{\mathbf{x}} = \mathbf{A}\Delta\mathbf{x} + \mathbf{B}\Delta\mathbf{u}, \tag{25} $$

where $\mathbf{A} = \left.\frac{\partial\mathbf{f}(\mathbf{x},\mathbf{u})}{\partial\mathbf{x}}\right|_{\mathbf{x}=\overline{\mathbf{x}},\mathbf{u}=\overline{\mathbf{u}}}, \mathbf{B} = \frac{\partial\mathbf{f}(\mathbf{x},\mathbf{u})}{\partial\mathbf{u}}$. Applying the LQR technique to the system (25), it is controllable as long as $\operatorname{rank}(\mathcal{C}(\mathbf{A},\mathbf{B})) = 9$, where $\mathcal{C}(\mathbf{A},\mathbf{B})$ is the controllability matrix of pair $(\mathbf{A},\mathbf{B})$. System (25) is discreted using the Tustin method. The state feedback controller is denoted as

$$ \mathbf{u} = \overline{\mathbf{u}} - \mathbf{K}\Delta\mathbf{x}, \tag{26} $$

where the gain matrix $\mathbf{K} \in \mathbb{R}^{4\times 9}$, obtained by solving an Discrete-time Algebraic Riccati Equation (DARE) with weight parameters $\mathbf{Q} \in \mathbb{R}^{9\times 9}$ and $\mathbf{R} \in \mathbb{R}^{4\times 4}$. However, it is worth noting that the rotors' thrust and servo angle are required by the state feedback controller (26). We could not obtain those states sometimes. A state predictor is adopted to address this problem, which is similar to *virtual control channels predictor* proposed in [16]. It can be expressed in the form of actuator dynamics, shown in Equ.(5) and Equ.(6). Thanks to the state predictor, the requirement for force and angle sensors is eliminated. Nevertheless, parameter mismatches could lead to errors in state prediction.

D. Postion Controller

In Section III-B and III-C , an LQR based reduced attitude controller is designed utilizing a relaxed hover solution. We combine reduced attitude control and position control to achieve control over spatial position of the failed bi-copter. Desired position $\mathbf{p}_{\mathrm{d}}$ is fed into the position controller, the desired average thrust direction ${}^{\mathrm{e}}\mathbf{n}_{\mathrm{d}}$ and desired acceleration $\mathbf{a}_{\mathrm{d}}$ are generated as the inputs of the reduced attitude controller. The position controller adopts a cascaded-PID controller. The desired acceleration $\mathbf{a}_{\mathrm{d}}$ is calculated by

$$ \begin{aligned} \mathbf{v}_{\mathrm{d}} &= \mathbf{K}_{\mathbf{p}_{\mathrm{p}}}(\mathbf{p}_{\mathrm{d}} - \mathbf{p}) + \mathbf{K}_{\mathbf{p}_{\mathrm{i}}}\int(\mathbf{p}_{\mathrm{d}} - \mathbf{p}) \\ \mathbf{a}_{\mathrm{d}} &= \mathbf{K}_{\mathbf{v}_{\mathrm{p}}}(\mathbf{v}_{\mathrm{d}} - \mathbf{v}) + \mathbf{K}_{\mathbf{v}_{\mathrm{i}}}\int(\mathbf{v}_{\mathrm{d}} - \mathbf{v}), \end{aligned} \tag{27} $$

where the vector $\mathbf{v}_{\mathrm{d}}$ is the desired velocity expressed in the Earth frame; matrices $\mathbf{K}_{\mathbf{p}_{\mathrm{p}}}, \mathbf{K}_{\mathbf{p}_{\mathrm{i}}}, \mathbf{K}_{\mathbf{v}_{\mathrm{p}}}, \mathbf{K}_{\mathbf{v}_{\mathrm{i}}} \in \mathbb{R}^{3\times 3}$ are parameters of the position controller. Furthermore, the desired *average thrust direction* is written as

$$ {}^{\mathrm{e}}\mathbf{n}_{\mathrm{d}} = -\frac{\mathbf{a}_{\mathrm{d}} - \mathbf{g}}{\|\mathbf{a}_{\mathrm{d}} - \mathbf{g}\|}. \tag{28} $$

Substituting $\mathbf{a}_{\mathrm{d}}$ into optimization problem (13) results in a new relaxed hover solution $\overline{\boldsymbol{\gamma}}$. With this, a new LQR gain matrix $\mathbf{K}$ can be solved, enabling the state feedback controller to stabilize the system towards the new desired acceleration $\mathbf{a}_{\mathrm{d}}$.

IV. Numerical Simulation and Analysis

In Section III, the relaxed hover solution is utilized for controller design. The entire control strategy is presented, including reduced attitude controller and position controller. This section focuses on its validation, the numerical simulations are conducted on Simulink [23].

A. Numerical Simulation Settings

The parameters of the bi-copter, obtained by identifying a real bi-copter, are given in Table. I. The problem (13) is solved with *sqp* [24] algorithm, and

$$ \begin{aligned} \mathbf{W}_1 &= \operatorname{diag}(100, 100, 5000), \mathbf{W}_2 = \operatorname{diag}(10, 10, 10), \\ \overline{\boldsymbol{\gamma}}_0 &= \begin{bmatrix}0\ 1\ -0.85\ -23.56\ -11.21\ 9.68\ 9.57\ 0\ 0.78\ 0\end{bmatrix}^{\mathrm{T}}, \\ \boldsymbol{\gamma}_{\min} &= \begin{bmatrix}-\pi\ -1\ -1\ -28\ -28\ -28\ 0\ 0\ \alpha_{\min,1}\ \alpha_{\min,2}\end{bmatrix}^{\mathrm{T}}, \\ \boldsymbol{\gamma}_{\max} &= \begin{bmatrix}\pi\ 1\ 1\ 28\ 28\ 28\ \lambda_1 T_{\max}\ \lambda_2 T_{\max}\ \alpha_{\max\,1}\ \alpha_{\max,2}\end{bmatrix}^{\mathrm{T}}. \end{aligned} $$

Note that the ϕ, θ and $\boldsymbol{\omega}$ should be appropriately constrained, and $\epsilon = 0.6$. The weight matrices $\mathbf{Q}$ and $\mathbf{R}$ are set as

$$ \begin{aligned} \mathbf{Q} &= \operatorname{diag}(4000, 4000, 40, 40, 40, 100, 100, 100, 100), \\ \mathbf{R} &= \operatorname{diag}(100, 100, 1000, 1000). \end{aligned} $$

TABLE I

PARAMETERS OF BI-COPTER

Parameter	Value
m(kg)	0.828
b(m)	0.14
h(m)	0.08
k_τ(m)	0.00778
τ_{m}(s)	0.03
τ_{s}(s)	0.02
$T_{\mathrm{max},i}$(N)	15
$\alpha_{\mathrm{min},i}$(rad), $\alpha_{\mathrm{max},i}$(rad)	-1.0472,1.0472
$\mathbf{J}$(kg $\cdot$ m^2)	diag(0.0084 , 0.0042 , 0.0063)
$\mathbf{k}_{\mathrm{air}}$(N/(rad/s))	diag(0.0012 , 0.0002 , 0.0008)
n_{gyro}(rad/s)	$\mathcal{N}(0, 0.01)$
n_{accel}(m/(s/s))	$\mathcal{N}(0, 0.1)$
n_{mag}(Gauss)	$\mathcal{N}(0, 0.02)$
n_{GPS}(m)	$\mathcal{N}(0, 0.1)$

For the position controller, its parameters are set as

$$\mathbf{K}_{\mathbf{p}_\mathrm{p}} = \mathrm{diag}\left(1,1,1\right), \mathbf{K}_{\mathbf{p}_\mathrm{i}} = \mathrm{diag}\left(0.05,0.05,0.05\right),$$
$$\mathbf{K}_{\mathbf{v}_\mathrm{p}} = \mathrm{diag}\left(2,2,2\right), \mathbf{K}_{\mathbf{v}_\mathrm{i}} = \mathrm{diag}\left(0.2,0.2,0.2\right).$$

To ensure the controller's robustness, the running frequency should be selected appropriately, the LQR controller's frequency should be higher than that of the position controller, due to its higher dynamics. Our control scheme is implemented with the position controller, which includes solving problem (13), running at 111Hz, while the reduced attitude controller operates at 333Hz. This frequency is limited by the Pulse Width Modulation (PWM) frequency of digital servos, typically 333Hz. Additionally, to simulate the actual bi-copter platform, sensors are also included, which are affected by additive Gaussian noise in the simulations, For these sensors, such as gyroscope, accelerometer, magnetometer, GPS, their noise characteristics are defined correspondingly in Table. I, and $n_{(\cdot)} \in \mathbb{R}$ represents the noise signal added to the sensors' ground truth. A state estimator [25] is employed to fuse sensors' data and provides information on position, velocity, and attitude. It runs at 999Hz, which is three times higher than the LQR controller's frequency, as determined by the sampling theorem [26]. Note that a first-order low-pass filter with a time constant of $\tau_{\mathrm{lpf}} = 0.04$ is applied to reduce the noise of solved $\overline{\gamma}$. A bi-copter plant is deployed at 2000Hz in numerical simulations. To demonstrate the effectiveness of the simulation, three cases are investigated. Specifically, for the case of servo stuck, the stuck angle should be chosen appropriately. When the bi-copters maneuver forward or backward, the servo instantaneously generates a significant tilt angle, aimed at producing pitch torque. The servos appear to be susceptible to failure. In this study, ± 0.5 rad is chosen as the stuck angles.

B. Case 1: Robustness Analysis of Rotational Damping

Rotational damping parameters, specifically the parameters of air drag $\mathbf{k}_{\mathrm{air}}$, as presented in Section II-A, have a significant impact on the stability of self-rotation [16]. Unfortunately, $\mathbf{k}_{\mathrm{air}}$ is often not precisely available due to aerodynamic factors. To verify the robustness subject to model uncertainty, Monte Carlo simulations are conducted with randomized rotational damping parameters $\mathbf{k}_{\mathrm{air}}$. According to Fig. 3, for all tests, our control scheme is able to account for the uncertainty in rotational damping parameters instead of resulting in a crash. An interesting phenomenon can be observed by comparing ${}^{\mathrm{e}}\mathbf{n}$ in (a) and (b). Clearly, $\epsilon = 1$ represents a constant initial solution for problem (13). Enabling of $\gamma_{\mathrm{feedback}}$ in the initial solution leads to better convergence of ${}^{\mathrm{e}}\mathbf{n}$, indicating a faster recovery. Therefore, the strategy (14) is beneficial for this FTC scheme.

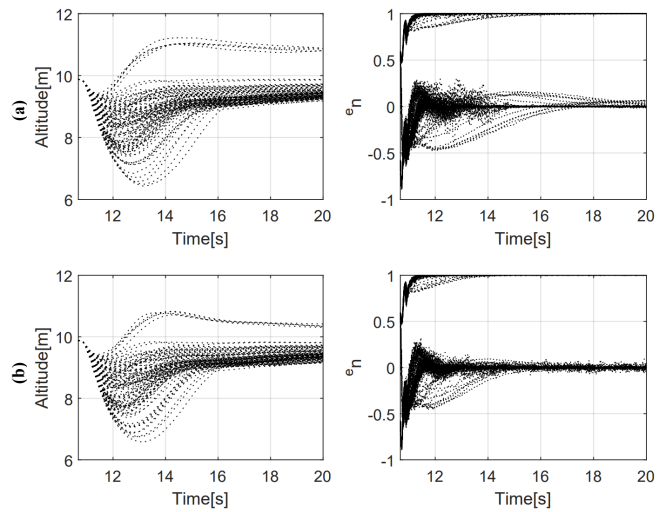

Fig. 3. The Altitude and ${}^{\mathrm{e}}\mathbf{n}$ Response of Monte Carlo Simulations with Randomized $\mathbf{k}_{\mathrm{air}}$: The bi-copter hovers at -10 meters with only the altitude controller enabled. Subsequently, $\lambda_2 = 0$ was injected, the loss of height and convergence of ${}^{\mathrm{e}}\mathbf{n}$ in the recovery process are depicted in this figure. 100 tests with randomized $\mathbf{k}_{\mathrm{air}}$, where $k_x \in [0.00024, 0.006]$, $k_y \in [0.00004, 0.001]$, $k_z \in [0.00016, 0.004]$, were conducted. For ϵ in the switching strategy (14), simulation results with $\epsilon = 1$ and $\epsilon = 0.6$ are displayed in Row (a) and Row (b). Note that both simulations (a) and (b) are performed with the same rotational damping parameters.

C. Case 2: Position Control with Complete Rotor Failure

To further ensure the effectiveness of the controller, simulations subject to complete rotor failure are performed first. The simulation results are shown in Fig. 4. After fault injection, to offset the torque generated by the single rotor, the bi-copter experiences self-rotation with a significant angular velocity to acquire gyro stability. Then, a stable ${}^{\mathrm{e}}\mathbf{n}$ is achieved. It is reasonable for the bi-copter with complete rotor failure to hover with rotor thrust slightly exceeding the bicopter's gravity. Note that the ${}^{\mathrm{e}}\mathbf{n}$ is disordered due to the almost-zero angular velocity within the green area. It is worth noting that the averaged force direction ${}^{\mathrm{e}}\mathbf{n}$ changes during the bi-copter maneuvers, aiming at trajectory tracking. Furthermore, when subjected to wind disturbances, the ${}^{\mathrm{e}}\mathbf{n}$ points towards the direction of x_{e}, and the tracking errors change slightly. As a result, Fig. 4 demonstrates that even with complete rotor failure, the bi-copter can perform position control robustly in the presence of wind disturbances using the proposed controller (specifically, $\lambda_2 = 0$).

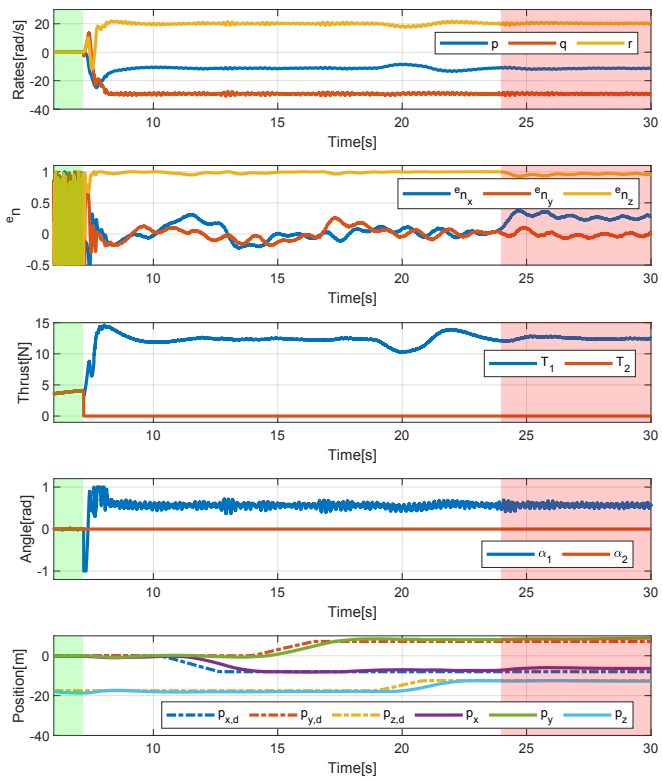

Fig. 4. Simulation of a Bi-copter with Complete Rotor Failure: The bi-copter hovers at approximately -18 meters, as shown in the green area. At 7 seconds, $\lambda_2 = 0$ is injected, after which the bi-copter tracks the desired trajectory. Additionally, a constant wind disturbance of $\mathbf{d}_{\text{linear}} = \begin{bmatrix} 2 & 0 & 0 \end{bmatrix}^{\text{T}}$ N is added along x_{e} within the red area.

D. Case 3: Position Control with Servo being Stuck at ± 0.5

The simulations with servo stuck failure are also conducted, as shown in Fig. 5. The servo is stuck at ± 0.5 rad, specifically $\alpha_2 = \alpha_{\text{min},2} = \alpha_{\text{max},2} = \pm 0.5$. The reference trajectory is set to be the same as that in *Case 2*. Similar phenomena are observed, such as the stabilization of $^{\text{e}}\mathbf{n}$. According to the results, the angular velocity in simulation (a) is notably larger than that in simulation (b), indicating a more stable spinning. Benefiting from the stable spinning, the averaged thrust direction $^{\text{e}}\mathbf{n}$, as shown in simulation (a), exhibits a smoother response during trajectory tracking compared to simulation (b). Furthermore, the thrusts in (a) and (b) differ significantly due to the opposite servo angle. The total thrust in (a) is larger than that in (b), indicating more energy is used for force counteraction and rotation promotion, which is inefficient. Therefore, the servo being stuck at -0.5 rad is more challenging than at $+0.5$ rad. Even so, Fig. 5 still indicates that the bi-copter using the proposed controller is capable of position control and robustness against wind disturbances despite the servo being stuck at ± 0.5 rad.

V. Discussion

In Section IV, numerical simulations are conducted. According to the simulation results, the objective of this study has been achieved. However, for experimental validations, much more effort should be invested. Real servos in bi-copters are typically nonlinear systems, but this study models them using a first-order model in simulation, which may significantly impact experimental results. Additionally, the gears of the servos are susceptible to wear during experiments, which may make the tests difficult to carry out. Therefore, designing a new FTC-friendly bi-copter is a pressing issue that requires immediate attention.

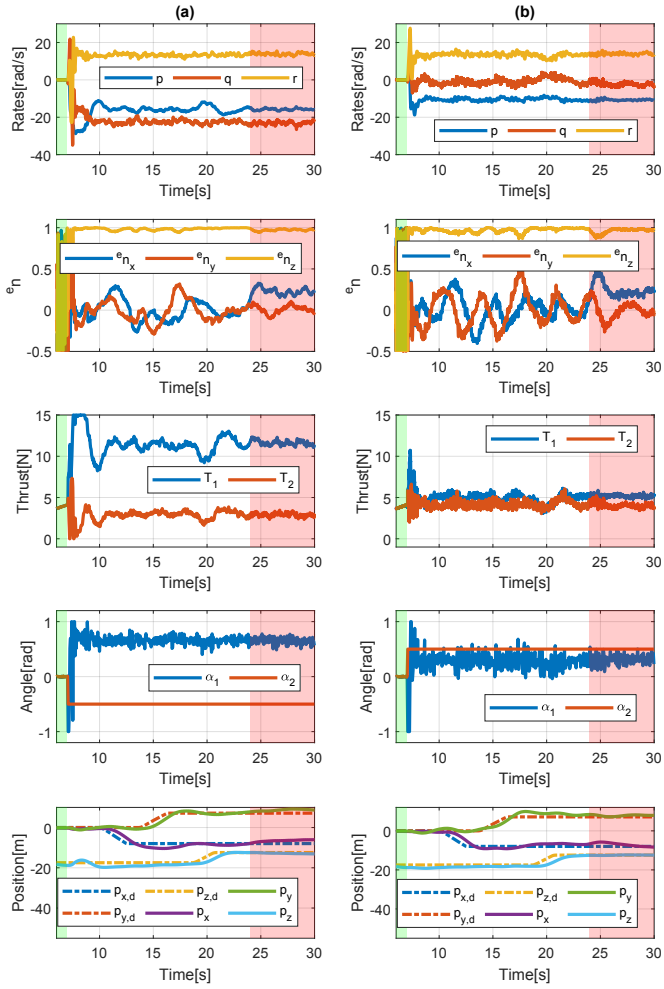

Fig. 5. Simulations of the Bi-copter with the Servo Stuck at -0.5rad and 0.5rad are Shown in Column (a) and Column (b): The bi-copter hovers at approximately -18 meters, as shown in the green area. At 7 seconds, the servo fault is injected, after which the bi-copter tracks the desired trajectory. Additionally, a constant wind disturbance of $\mathbf{d}_{\text{linear}} = \begin{bmatrix} 2 & 0 & 0 \end{bmatrix}^{\text{T}}$ N is also added along x_{e} within the red area.

VI. Conclusion and Future Work

This study has designed a relaxed hover solution based control scheme for bi-copters subject to rotor or servo stuck failure. Numerical simulations were conducted to validate the effectiveness of the control scheme. Its robustness to constant wind disturbance and rotational damping uncertainty was also evaluated. In future work, building upon this study, our focus will be on designing bi-copters and conducting real-flight experiments.

REFERENCES

[1] Q. Quan, *Introduction to Multicopter Design and Control*. Springer, 2017.

[2] X. Qi, D. Theilliol, J. Qi, Y. Zhang, and J. Han, "A literature review on fault diagnosis methods for manned and unmanned helicopters," in *2013 International Conference on Unmanned Aircraft Systems (ICUAS)*, 2013, pp. 1114–1118.

[3] W. Hao, B. Xian, and T. Xie, "Fault-tolerant position tracking control design for a tilt tri-rotor unmanned aerial vehicle," *IEEE Transactions on Industrial Electronics*, vol. 69, no. 1, pp. 604–612, 2022.

[4] R. Venkataraman, P. Seiler, M. Lukátsi, and B. Vanek, "Reliability assessment of actuator architectures for unmanned aircraft," *Journal of Aircraft*, vol. 54, no. 3, pp. 955–966, 2017.

[5] S. Park, J. Bae, Y. Kim, and S. Kim, "Fault tolerant flight control system for the tilt-rotor UAV," *Journal of the Franklin Institute*, vol. 350, no. 9, pp. 2535–2559, 2013.

[6] H. Bhardwaj, X. Cai, S. K. H. Win, and S. Foong, "Design, modeling and control of a two flight mode capable single wing rotorcraft with mid-air transition ability," *IEEE Robotics and Automation Letters*, vol. 7, no. 4, pp. 11 720–11 727, 2022.

[7] A. S. Saeed, A. B. Younes, S. Islam, J. Dias, L. Seneviratne, and G. Cai, "A review on the platform design, dynamic modeling and control of hybrid UAVs," in *2015 International Conference on Unmanned Aircraft Systems (ICUAS)*, 2015, pp. 806–815.

[8] Y. Qin, W. Xu, A. Lee, and F. Zhang, "Gemini: A compact yet efficient bi-copter UAV for indoor applications," *IEEE Robotics and Automation Letters*, vol. 5, no. 2, pp. 3213–3220, 2020.

[9] M. W. Mueller and R. D'Andrea, "Relaxed hover solutions for multicopters: Application to algorithmic redundancy and novel vehicles," *The International Journal of Robotics Research*, vol. 35, no. 8, pp. 873–889, 2016.

[10] C. Ke, K.-Y. Cai, and Q. Quan, "Uniform passive fault-tolerant control of a quadcopter with one, two, or three rotor failure," *IEEE Transactions on Robotics*, vol. 39, no. 6, pp. 4297–4311, 2023.

[11] F. Nan, S. Sun, P. Foehn, and D. Scaramuzza, "Nonlinear mpc for quadrotor fault-tolerant control," *IEEE Robotics and Automation Letters*, vol. 7, no. 2, pp. 5047–5054, 2022.

[12] J. I. Giribet, R. S. Sanchez-Pena, and A. S. Ghersin, "Analysis and design of a tilted rotor hexacopter for fault tolerance," *IEEE Transactions on Aerospace and Electronic Systems*, vol. 52, no. 4, pp. 1555–1567, 2016.

[13] L. J. Colombo and J. I. Giribet, "Learning-based fault-tolerant control for an hexarotor with model uncertainty," *IEEE Transactions on Control Systems Technology*, vol. 32, no. 2, pp. 672–679, 2024.

[14] W. Zhang, M. W. Mueller, and R. D'Andrea, "Design, modeling and control of a flying vehicle with a single moving part that can be positioned anywhere in space," *Mechatronics*, vol. 61, pp. 117–130, 2019.

[15] W. Zhang, M. W. Mueller, and R. D'Andrea, "A controllable flying vehicle with a single moving part," in *2016 IEEE International Conference on Robotics and Automation (ICRA)*, 2016, pp. 3275–3281.

[16] C. Ke, K.-Y. Cai, and Q. Quan, "Uniform fault-tolerant control of a quadcopter with rotor failure," *IEEE/ASME Transactions on Mechatronics*, vol. 28, no. 1, pp. 507–517, 2023.

[17] R. I. Leine, G. Capobianco, P. Bartelt, M. Christen, and A. Caviezel, "Stability of rigid body motion through an extended intermediate axis theorem: application to rockfall simulation," *Multibody System Dynamics*, vol. 52, no. 4, pp. 431–455, 2021.

[18] M. W. Mueller and R. D'Andrea, "Stability and control of a quadrocopter despite the complete loss of one, two, or three propellers," in *2014 IEEE International Conference on Robotics and Automation (ICRA)*, 2014, pp. 45–52.

[19] B. A. S. van Schijndel, S. Sun, and C. De Visser, "Fast loss of effectiveness detection on a quadrotor using onboard sensors and a kalman estimation approach," in *2023 International Conference on Unmanned Aircraft Systems (ICUAS)*, 2023, pp. 1–8.

[20] B. Ghalamchi, Z. Jia, and M. W. Mueller, "Real-time vibration-based propeller fault diagnosis for multicopters," *IEEE/ASME Transactions on Mechatronics*, vol. 25, no. 1, pp. 395–405, 2020.

[21] M. D. Shuster, "A survey of attitude representations," *Navigation*, vol. 8, no. 9, pp. 439–517, 1993.

[22] D. P. Bertsekas, "Dynamic programming and optimal control," *Athena Scientific*, 1995.

[23] Mathworks.com, "Simulink," https://www.mathworks.com/products/simulink.html, accessed: March 6, 2024.

[24] ——, "Choosing the algorithm," https://www.mathworks.com/help/optim/ug/choosing-the-algorithm.html, accessed: March 6, 2024.

[25] R. Mahony, T. Hamel, and J. M. Pflimlin, "Nonlinear complementary filters on the special orthogonal group," *IEEE Transactions on Automatic Control*, vol. 53, no. 5, pp. 1203–1218, 2008.

[26] K. Ogata, *Discrete-time Control Systems*. Prentice Hall, 1995.